Green Chemistry

COMMUNICATION

View Article Online
View Journal | View Issue

Cite this: *Green Chem.*, 2017, **19**, 5575

Received 14th July 2017,
Accepted 25th October 2017

DOI: 10.1039/c7gc02139a

rsc.li/greenchem

A dual-templating strategy for the scale-up synthesis of dendritic mesoporous silica nanospheres†

Peng-Cheng Liu,‡ Ye-Jun Yu,‡ Bo Peng, Shi-Yu Ma,* Tian-Yu Ning, Bing-Qian Shan, Tai-Qun Yang, Qing-Song Xue, Kun Zhang * and Peng Wu *

We have demonstrated a facile and green way to synthesize dendritic mesoporous silica nanoparticles (DMSNs) on an ultra-large scale (kg) with cetyltrimethylammonium bromide (CTAB) and an anionic surfactant as dual templates free of organic solvents. In contrast to its co-template role in tuning the packing parameter of the surfactant molecule organization, the anionic surfactant herein acts as a more strongly competitive counterion against the adsorption of negatively charged silicate oligomers (I^-) on the micelles. Based on the new understanding of the interaction between the cationic–anionic surfactant ionic pairs and the silicate oligomers, we proposed a dual template synergistically controlled micelle self-aggregated model to understand the formation mechanism of dendritic MSNs where the anionic surfactant stabilized micelles or micelle blocks are basic self-assembling building units for the formation of center-radial pore channel networks. By using one-pot *in situ* isomorphous substitution, the metal Ti atom can be easily incorporated into the silica frameworks of DMSNs, and the obtained Ti-DMSN catalyst shows a superior catalytic performance in the epoxidation of cyclohexene over the typical mesoporous Ti-MCM-41 silicas.

Green and large scale production of mesoporous nanoparticles with a controlled particle size and morphology is highly regarded for applications in nanomedicine, optical devices, batteries, heterogeneous catalysts and nanofiltration. In particular, dendritic mesoporous silica nanoparticles (DMSNs) with center-radial oriented open and large mesopores have attracted much more attention in recent years because of their unique open three-dimensional superstructures with high accessibility to the internal surface areas.[1–10] However, due to the complex dynamic self-assembly of abundant silicate species and surfactants occurring on the unstable nano-scale interfaces of micelles, the reproducible scale-up synthesis of discrete and highly dispersed dendritic mesoporous silica nano-spheres (DMSNs) with diameters below 150 nm is extremely difficult by conventional solo surfactant soft-templating methods and remains a great challenge.

Recently, based on some in-depth understanding of the nucleation and growth mechanism of mesoporous silica nanoparticles (MSNs), several research groups, including us, have successfully realized the synthesis of dendritic silica nanospheres with centre-radial pore channels using the classical micro-emulsion approach (also called the biphasic stratification approach, therein, a large quantity of volatile organic solvents is widely used, such as cyclohexane and ether),[11–17] the organosilane assisted co-condensation method,[18–20] the dynamic polystyrene template method[21] and our interfacial counterion induced self-assembly process of spherical micelles.[22,23] However, these synthetic strategies are still very limited and have some disadvantages, such as the use of a large quantity of non-environmentally benign cationic surfactants and organic solvents, lack of continuity and flexibility in their size and morphology control, and a low final yield (generally on the gram scale). Interestingly, it is worth noting that, so far, only a solo cationic surfactant has been used as a template for the synthesis of DMSNs. It is known from the chemistry of surfactants that various shapes and morphologies of surfactants, *e.g.*, micelles, vesicles and liquid crystal phases can be formed in dual surfactant solutions with a low concentration relative to that of one surfactant solution.[5] In dual template systems, the anionic surfactant usually plays a co-template role in tuning the packing parameter (g) of the surfactant molecule organization ($g = V/al$, where V is the effective volume of the surfactant tail region, a refers to the effective head-group area on the micelle surface, and l is the surfactant tail length). Therefore, a so-called dual-template (or co-template) route has become the focus of the controlled synthesis of mesoporous silicas with varied morphologies.[24–26] Yeh and his coworkers first reported the synthesis of hollow silica spheres with a mesostructured shell using cationic–anionic–neutral block

---

Shanghai Key Laboratory of Green Chemistry and Chemical Processes, School of Chemistry and Molecular Engineering, East China Normal University, No. 3663, North Zhongshan Rd., Shanghai 200062, P.R. China. E-mail: syma@chem.ecnu.edu.cn, pwu@chem.ecnu.edu.cn, kzhang@chem.ecnu.edu.cn

† Electronic supplementary information (ESI) available. See DOI: 10.1039/c7gc02139a

‡ These authors contributed equally to this research.

copolymer ternary surfactants as templates,[27] followed by other research groups.[28,29] So far, the successful synthesis of dendritic MSNs by a dual-templating strategy has not been reported.

As expected, by changing the concentration of dual surfactants of cetyltrimethylammonium bromide (CTAB) and anionic sodium dodecyl sulfate (SDS) surfactant which acted as co-templates, at a high concentration, we facilely achieved the synthesis of silkworm cocoon-like and mono-lamellar vesicle structured mesoporous silica nanoparticles (called SW-MSNs and V-MSNs hereafter, respectively); to our big surprise, at a very low concentration of dual surfactants in pure water solution (free of organic solvents), an ultra-large-scale synthesis of dendritic mesoporous silica nanospheres (DMSNs) with *ca.* 100 nm size on the kg scale was first demonstrated to the best of our knowledge. Completely different from the conventional view on the role of an anionic surfactant in the mixed surfactant system tuning the packing parameter (g) of the surfactant molecule organization, in the current synthesis it acts as a more strongly competitive counterion against the adsorption of negatively charged silicate oligomers (I^-) on the inorganic–organic electrical interface of a mixed surfactant micelle to form micelles or micelle blocks partially covered with silica. The anionic surfactant stabilized micelles or micelle blocks are basic self-assembly building units for the formation of centre-radial pore channel networks. It is very interesting that the metal Ti atoms can be easily incorporated into the silica frameworks of DMSNs by *in situ* isomorphous substitution, and the obtained Ti-DMSN catalyst shows a superior catalytic performance in the epoxidation of cyclohexene with *tert*-butyl hydroperoxide (TBHP) as an oxidant over classical microporous TS-1 zeolites and mesoporous Ti-MCM-41 silica.

The mesoporous materials with varied morphologies were prepared in basic solution using the cationic surfactant cetyltrimethylammonium bromide (CTAB) and an anionic surfactant as co-templates with varied concentrations and molar ratios in the presence of tetraethoxysilane (TEOS) as a silica source (for experimental details see the ESI†). The samples were designated as DMSNs, SW-MSNs, V-MSNs and MSNs, corresponding to their own dendritic, silkworm cocoon-like, mono-lamellar vesicle structured and spherical morphology, respectively (Fig. 1). Fig. 1 shows the SEM and TEM images of representative mesoporous silica nanoparticles (MSNs) with varied morphologies synthesized by using dual CTAB, sodium dodecyl sulfate (SDS) templates and a single CTAB template. When the molar ratio of (CATB + SDS)/TEOS is set to a higher value of 0.18, silkworm cocoon-like (Fig. 1c and d) and mono-lamellar vesicle structured (Fig. 1e and f) MSNs were formed, and at a high base concentration, the vesicular nanostructured spheres with a size of *ca.* 250 nm were preferentially obtained. The formation mechanism of SW-MSNs, V-MSNs can be explained by a geometric packing model of surfactant chemistry.[24] The interaction between anionic SDS and CTA^+ at the interface of a micelle may counteract part of the cationic charges in the CTA^+ molecules, and thus a is decreased. Therefore, the resulting larger g factor induced the formation of SW-MSNs and V-MSNs. It also answers that, in our case, at a higher concentration of the base, V-MSNs with a mono-lamellar vesicular structure and with larger g factors are preferentially prepared.

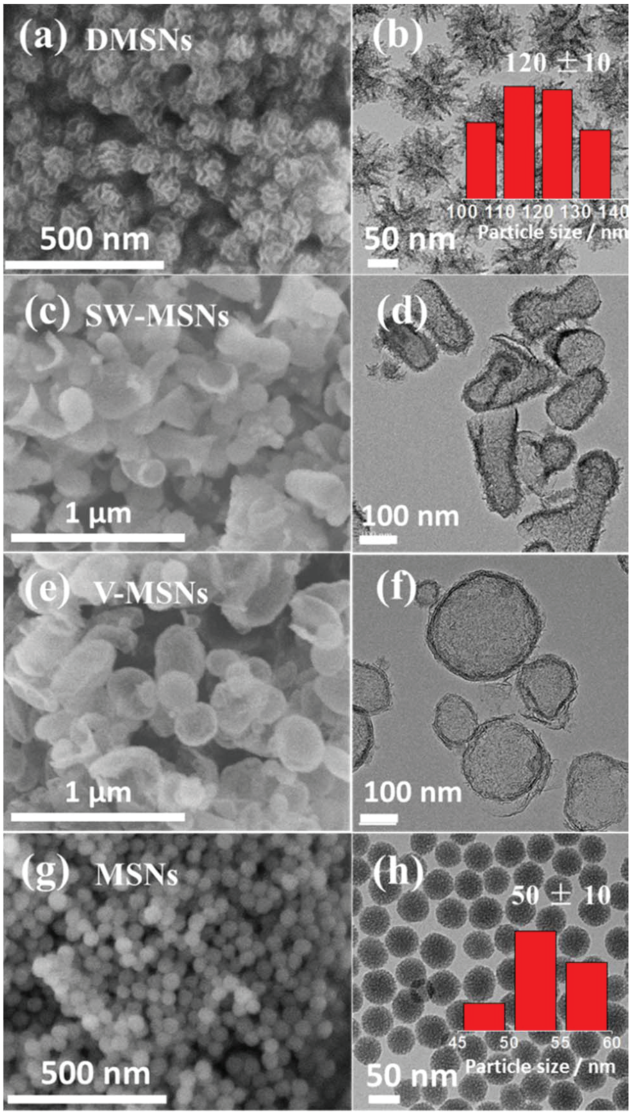

Fig. 1 SEM and TEM images of dendritic (a, b), silkworm cocoon-like (c, d), mono-lamellar vesicle structured (e, f) and spherical (g, h) mesoporous silica nanoparticles synthesized by using dual templates CTAB + SDS (a–f) and a solo surfactant CTAB (g, h), respectively. Particle size (PS) histograms obtained from the TEM pictures on N particles are (N > 100 in each case) provided as the inserts of a and g.

Unexpectedly, at low concentrations of CTAB and SDS with an ultra-low molar ratio of (CATB + SDS)/TEOS of 0.08, the uniform dendritic mesoporous silica nanospheres (DMSNs) with a size of *ca.* 120 nm were synthesized (Fig. 1a and b). The TEM images in Fig. 1b indicate that the pores are radially oriented, and the nanoparticles are homogeneously distributed without any aggregation. By simply adjusting the reaction conditions, such as the types of anionic surfactants (Fig. 2), the carbon chain lengths of the main cationic surfactants (Fig. S1†), the base source (Fig. S2†), and the particle size of DMSNs can be easily tuned from 50 nm to 150 nm (Table S1†). However, if only a single surfactant CTAB was used as a template, the regular monodisperse mesoporous silica nanospheres (MSNs) with a smaller particle size (*ca.* 50 nm) and a unique pore size distribution were obtained (Table S1†).[30] All the samples exhibit a typical IV isotherm with a hysteresis loop in the relative pressure range of 0.2–1.0 implying the presence of mesopores (Fig. 3 and Fig. S3†). It is worth noting that DMSNs have bimodal pore size distributions: one is *ca.* 3 nm obtained from the single micelle formed by mixed cationic and anionic surfactants similar to that of conventional MSNs, and the other broad mesopore centered at 10–12 nm originates from the aggregated micelle blocks, confirming the nature of the hierarchical porosity of dendritic mesoporous silica nanoparticles. The obtained DMSNs by using the dual templating strategy exhibit a high surface area (450 m^2 g^{-1}) and a large pore volume (1.59 cm^3 g^{-1}).

It is intriguing to note that, at a constant concentration of the anionic surfactant, even the chemical structure of the hydrophilic head of an anionic surfactant was changed and the morphology and dendritic channel network of MSNs were not varied (Fig. 2), implying that the dual-templating strategy is a versatile and general protocol for the synthesis of dendritic MSNs. Among the selected anionic surfactants, sodium dodecyl benzene sulfonate (SDBS), sodium dodecyl sulfate (SDS), sodium laurate (SL) and sodium stearate (SS), in view of green synthesis, the nontoxic and the most easily available sodium stearate is the best candidate for the large scale synthesis of DMSNs since the purified sodium stearate can be readily prepared by neutralizing the biomass resource stearic acid with sodium hydroxide. The use of environment-friendly chemicals and subsequent facile recovery allowed a high yield production on the kilogram scale. This novel technique has possible practical applications in industry as a catalyst support in the near future.

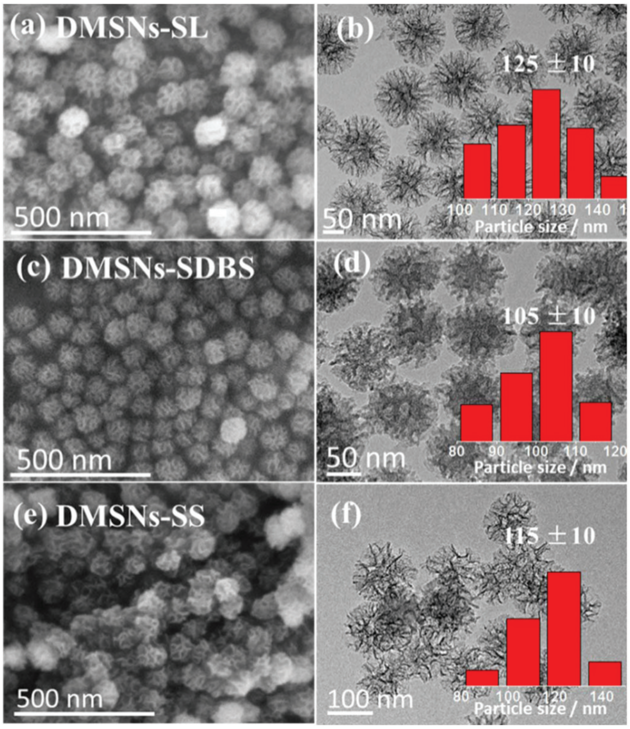

Fig. 2 SEM and TEM images of DMSNs synthesized by CTAB + SL (a, b) and CTAB + SDBS (c, d) and CTAB + SS (e, f). SL, SDBS and SS correspond to different anionic surfactants, sodium laurate, and sodium dodecyl benzene sulfonate and sodium stearate, respectively.

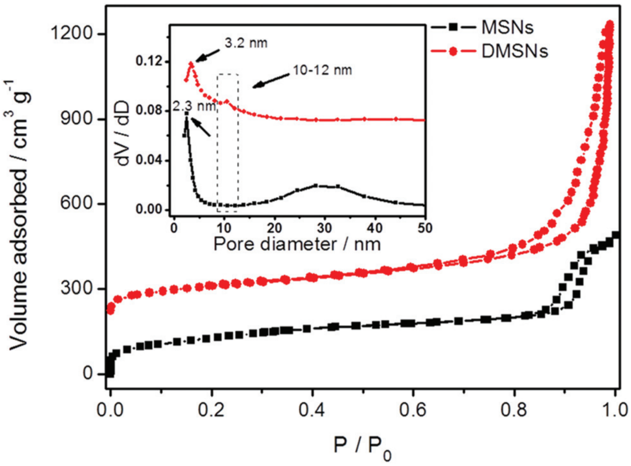

Fig. 3 N_2 adsorption–desorption isotherms and pore size distribution calculated by using the BJH model (insert) of DMSNs and MSNs synthesized by using dual templates of CTAB + SDS and a single template of CTAB, respectively. DMSNs show the typical hierarchical pore structure with bimodal pore size distributions, instead of the unique pore size distribution of the conventional MSNs (isotherms offset vertically by 200 cm^3 g^{-1} consecutively).

To preclude the salt effect of anionic surfactants on the detailed internal mesostructures of the silica nanoparticles, sodium sulfate (Na_2SO_4) or sodium methanesulfonate ($NaSO_3$–CH_3) as a replacement for the long chain anionic surfactant was also added to understand the formation mechanism of dendritic MSNs. The addition of these inorganic mineralization agents only accelerates the growth rate of nanoparticles, leading to the formation of regular mesoporous nanospheres with a larger particle size (Fig. S4†), instead of dendritic MSNs with center-radial pore channel networks. Obviously, the anionic surfactants with a long carbon chain are a requisite for the synthesis of DMSNs. The IR spectrum (Fig. S5†) and thermogravimetric (TG, Fig. S6†) analyses prove the presence of anionic surfactants in the micelles of DMSNs, indicating that the anionic surfactant is involved in the self-assembly process of silicates and micelle templates. In our previous report,[22] we showed that the existence of a strongly binding counterion (Tos^-) of the surfactant plays a critical role in the formation of micelle blocks, which induces the final stellate pore network. In the current synthesis, the anionic surfactant has a much higher affinity than the Tos^- anion for the electrical palisade of the CTA^+ micelles due to the very strong hydrophobic forces between the long carbon chains. The presence of the anionic surfactant in the mixed surfactant micelles strongly counteracts the competitive adsorption of silicate oligomers (I^-) on the CTA^+ micelles due to the electrostatic repulsion relative to the single cationic CTA^+ micelles. Thus, during the nucleation and growth process, anionic surfactant-stabilized micelle blocks or aggregates are formed and used as templates to generate the radial mesopores of DMSNs.

It should be mentioned that, when the chain length of the main cationic surfactant was changed, the dendritic morphology was reserved except for the particle size, and we found that the longer the chain of the main surfactant, the smaller the particle size (Fig. S1†). At a constant concentration of the surfactant, the longer the chain, the smaller value of CMC of the surfactant. Thus, more micelles lead to the smaller particle size, indicating that the nucleation of DMSNs is a spherical micelle aggregated kinetic process. When the organic triethanolamine ($TEAH_3$, $pK_a = 7.8$) is changed to an inorganic base, such as ammonia ($pK_a = 9.2$) and sodium hydroxide (strong electrolyte), the particle size is decreased further. When sodium hydroxide was used, the dendritic mesoporous silica nanospheres with the smallest particle size of *ca.* 55 nm were first prepared. It is well known that the larger pK_a increases the pH of the reaction system and accelerates the nucleation rate, and finally produces smaller nanoparticles indicating that the nucleation and growth of MSNs is a spherical micelle aggregation induced kinetic process again.[31]

The physisorption measurement and electron microscopy observation provide direct evidence that the open 'V' shaped pore networks in dendritic MSNs are interconnected by small, intermediate, and large pores (Fig. 4). This is the reason that dendritic MSNs are also called pore-expanded or hierarchical pore structured mesoporous silica nanoparticles.[5,9] But an elusive and important question had come up with the origin of this unique hierarchical porosity. If the material under investigation is purely mesoporous and contains non-intersecting mesopores of a cylindrical geometry and similar sizes like those in MCM-41 or SBA-15 (Fig. 4, inset 2), both from a historical and thermodynamic points of view, the desorption branch in these cases is often favoured to derive mesopore size distributions from the isotherm. However, currently synthesized dendritic MSNs have a very unique radial 'V' shape channel (TEM images in Fig. 1b, 2b, d, f and 4). Due to the pore network effects as shown in Fig. 4 (inset 1),[32–34] the adsorption branch is highly preferred for pore size calculations. Indeed, the pore network in our dendritic MSNs is very similar to the model of the pore network in the amorphous silica sol particles (Fig. 4, inset 1).

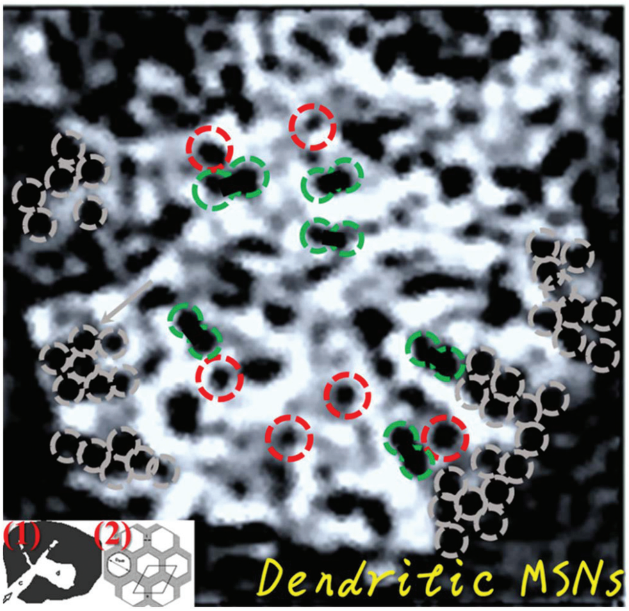

Fig. 4 Pore networks of the typical dendritic MSNs by TEM observation. Red, green and brown circles indicate the small, intermediate and large pores using monomicelles, bimicelles and aggregated micelles as the template or structure building units, respectively. (Inset 1, pore networks of classical amorphous silica sol particles; Inset 2, the hexagonal pore array of MCM-41 or SBA-15.)

To explore the origin of the hierarchical porosity of DMSNs, the pore size distribution (PSD) of typical dendritic MSNs is demonstrated by the calculation using the BJH method from both adsorption and desorption branches with different scales of the vertical axis of dV/dD and $dV/d\log(dp)$ as shown in Fig. 5 and Fig. S7,† respectively. Due to the presence of a large quantity of packing voids of inter-nanoparticles, a very broad pore size distribution centred at 40 nm is observed in both adsorption and desorption branches with the scale of the vertical axis of $dV/d\log(dp)$ as shown in Fig. S7.† Because of the overlapping with the inter-nanoparticle packing porosity, the intrinsic hierarchical mesopores in the dendritic MSNs are not readily distinguished. However, when the scale of the vertical axis is changed to dV/dD, the pore size distribution of the dendritic MSNs exhibits a multi-model distribution with a pore size centred at *ca.* 4.0, 20 and 40 nm, which corresponds to small, intermediate and large pores in the model as shown in Fig. 5, respectively. Obviously, the latter calculation by the BJH method from the adsorption branch provides a more reliable picture of the actual pore system as evidenced by SEM and TEM observation. Thus, for the proper interpretation of the adsorption data, especially for pore size calculations in the novel mesostructures, the shape of the isotherm (both adsorption and desorption branches) including the hysteresis loop should be taken into consideration. From these characterization methods, we can deduce that the monomicelles, bimicelles and aggregated micelles partially covered by silicate oligomers are the primary building units for the final nanospheres. We provide direct evidence that the dendritic MSNs are formed by the disordered self-assembly of these building units, differing from the conventional synergetic self-assembly process of MCM-41 and SBA-15.

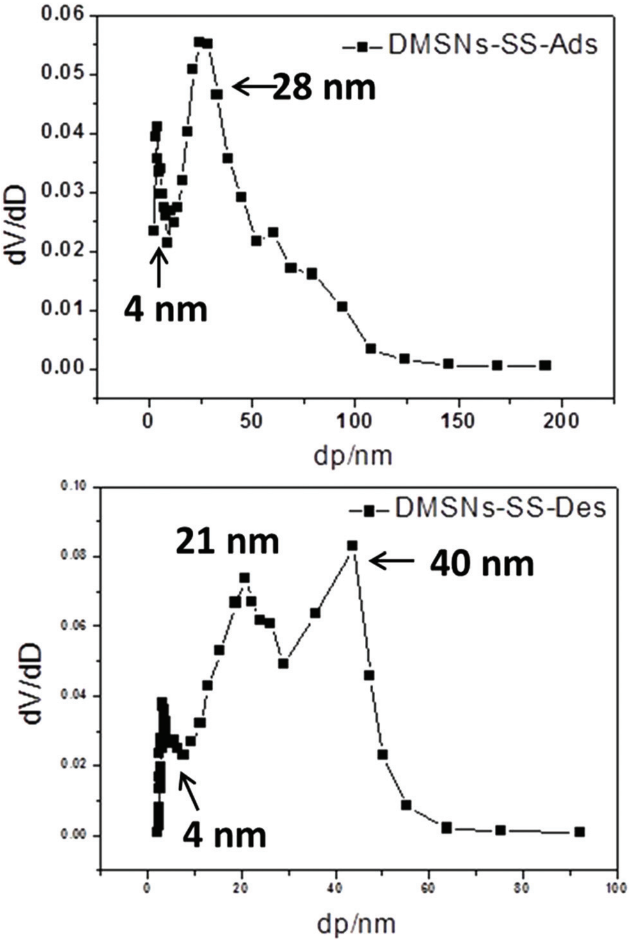

Fig. 5 Pore size distribution (PSD) of typical dendritic MSNs synthesized by using the dual-templating strategy in the presence of the anionic sodium stearate (SS) surfactant calculated by the BJH method from both adsorption and desorption branches.

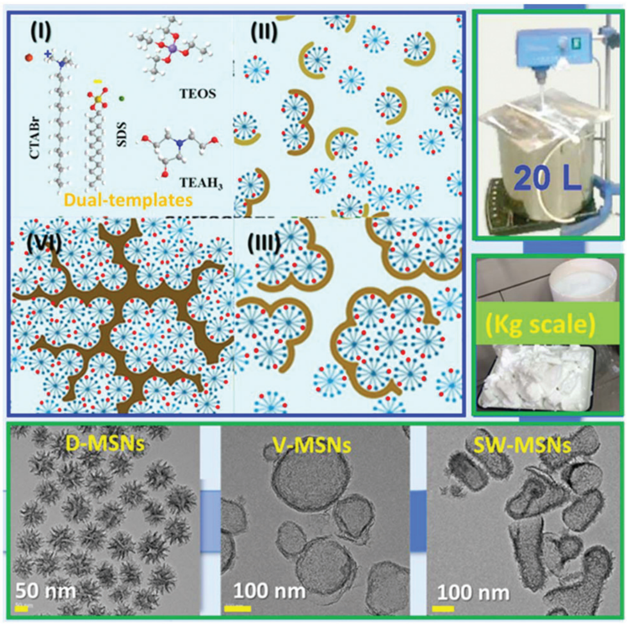

Scheme 1 Dual template synergistically controlled micelle self-aggregated model to understand the formation mechanism of dendritic MSNs.

According to the results discussed above, a dual template synergistically controlled micelle self-aggregated model was proposed to understand the formation mechanism of dendritic MSNs (Scheme 1). In the first step, due to the strong hydrophobic interaction between anionic surfactant carbon chains, the anionic and cationic mixed micelles are formed. Therein, the anionic surfactant is not used as a co-template to form the complicated surfactant aggregates. It just acts as a counterion against the adsorption of negatively charged silicate oligomers (I^-) on the inorganic–organic electrical interface of mixed micelles. Due to the hydrolysis and condensation of TEOS under basic conditions, the mono micelle partially coated with silica is formed in the second step. These specific anionic surfactant stabilized micelles can then fuse to form micelle blocks or aggregates in order to minimize the interface energy, which are nuclei for the growth of the final nanoparticles in the third step. The monomicelles, bimicelles and aggregated micelles partially covered by silicate oligomers in II and III steps are the building units for the final nanospheres. For the dendritic channel, you can imagine that the spherical pores with open windows are encapsulated in the bell mouth (conical hole). In the final step, the aggregation of micelle blocks induces the final dendritic pore channel networks. In the model, the anionic surfactant stabilized micelles or micelle blocks are key self-assembling building units for the formation of centre-radial pore channel networks.

Even though several successful synthetic routes were reported for the synthesis of dendritic MSNs, of course including the normal MSNs. Major drawbacks remain, namely, the use of low silica concentrations, large reaction volumes, large quantities of organic solvents, and poor nanoparticle yields.[35,36] Our developed dual-templating strategy demonstrates a high synthesis efficiency with a high yield (*ca.* 92%). By using a simple calculation of material balance based on the TG analysis (Fig. S6†), the utilization of dual-templates is 98.9%, and the leaching of the silica source is only 9.6% (in fact, the silicate species in the solution can be 100% recovered). Very importantly, the very low molar ratio of water/silica of 80 in the gel composition significantly decreases the use of water, in turn, increases the solid content of the slurry. Both advantages release the environmental burden of wastewater discharges. The high yield production of the final nanoparticles related to the hydrolysis and condensation chemistry of TEOS can be easily understood. We measured the pH evolution of the reaction system. At the starting point of the reaction, the pH is high, close to 11.0, which benefits the hydrolysis of TEOS. With the reaction evolution, the pH is slowly decreased to *ca.* 7.0. It is well known that under neutral conditions, the condensation rate of silicate species is maximum.[2] Thus, the utilization of silica is significantly increased which leads to a high yield of the final products. The pH evolution of the reaction system is probably related to the effective incorporation of Ti atoms into the silica frameworks by matching the condensation rate of silica and metal oxide later.[37] In addition, the synthetic compositions (*i.e.*, a low solid/solution ratio and extremely low surfactant and base concentrations) and mild conditions (*i.e.*, T = 80 °C and final pH = 7.0) are close to those of the silicification environment for diatom formation. This dual-surfactant templating method firstly provides the possibility to perform "green" syntheses of MSNs on a large scale.

Dendritic mesoporous silica nanoparticles with centre-radial pore structures have attracted considerable attention owing to their unique open three-dimensional dendritic super-structures with large pore channels and highly accessible internal surface areas compared with the conventional microporous zeolites and mesoporous silica (MCM-41 and SBA-15). Herein, the Ti-containing DMSNs (Ti-DMSNs) were compared with the benchmark heterogeneous microporous TS-1 catalysts and classical Ti-MCM-41 catalysts in the catalytic liquid epoxidation of olefins for bulky organic substrates.[38] In the pioneering work performed through fine tuning of the matching condensation rate of silica and metal oxide, Lin and his coworkers first reported the preparation of nano-sized mesoporous silicas with heterometal incorporation *via* a two-step synthetic process.[37] Inspired by these findings, by a similar isomorphous substitution, we synthesized Ti incorporated dendritic mesoporous silica nanospheres (Ti-DMSNs) by using our developed one-pot dual-template method. The SEM and TEM observation shows that the morphology of DMSNs is not varied due to Ti incorporation (Fig. 6a and b). In the UV-visible spectrum (Fig. 6c), Ti-DMSNs show the main absorption peak around 230 nm similar to Ti-MCM-41 (Fig. S8†), which is assigned to the charge transfer from O^{2-} to Ti^{4+}, indicating that the tetrahedrally coordinated Ti atoms are highly dispersed in the silica framework.[38,39] As shown in Table 1, the cyclohexene epoxidation reaction is highly selective and independent of titanosilicates (>95%). The Ti-DMSNs with more open dendritic pores show the maximum chemical reactivity with a CHO yield of 25.1%, even higher than that of Ti-MCM-41 (22.9%). The higher catalytic performance of Ti-DMSNs over Ti-MCM-41 is probably related to the high dispersion of tetrahedrally coordinated Ti atoms in the silica frameworks under our unique synthetic conditions with the final pH of *ca.* 7.0, which matches the condensation rate of silica and metal oxide. The chemistry of Ti in porous materials is very complicated. An in-depth understanding of the precise location and coordination environment of Ti atoms in the confined nanospace is needed for further investigation. By contrast, the TS-1 catalyst with micropores (Fig. S9†) is much less active, showing an extremely low PO yield (0.2%). After the fourth reuse of Ti-DMSNs, the chemical reactivity has only slightly decreased (Fig. 6d), indicating that the Ti-DMSN catalyst synthesized by the dual-templating strategy is a stable and robust catalyst. This clearly shows that wide-open dendritic pore channels are more favorable for catalysis especially for large molecules, as they minimize the molecular diffusion-limitation.

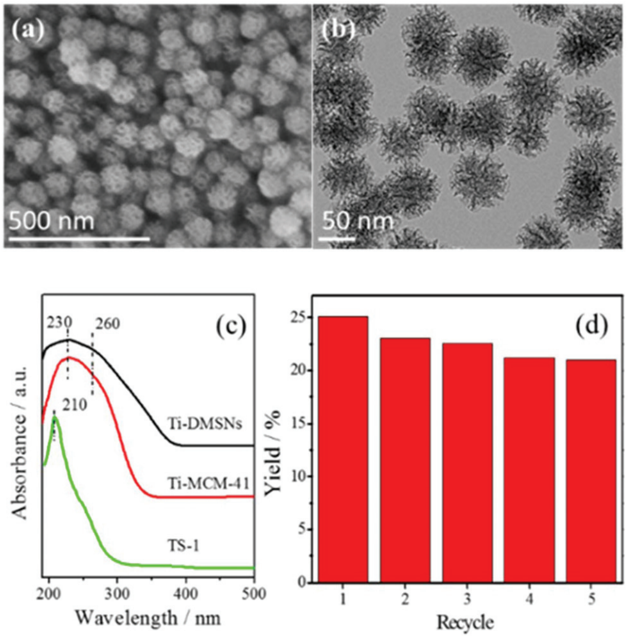

Fig. 6 SEM and TEM images (a, b) of Ti-DMSNs, UV-vis spectra (c) of different catalysts and the reuse of the epoxidation of cyclohexene on Ti-DMSNs (d).

In summary, we have discovered a facile and large scale approach to finely control the synthesis of mesoporous silica nanoparticles with different morphologies, including nanospheres, silkworm cocoon-like nanoshapes and mono-lamellar nanovesicles by tailoring the molar ratio of dual cationic and anionic surfactants (SDS and CTAB). At a ultra-low concentration of dual templates, we achieved the synthesis of dendritic mesoporous silica nanospheres (DMSNs) with a high yield (86.3%) on a large scale (kilograms). The obtained dendritic mesoporous silica nanospheres have a high surface area (*ca.* 450 m^2 g^{-1}) and large pore volume (1.60 cm^3 g^{-1}). The particle size of the DMSNs is uniform and easily tuneable from 50 to 150 nm by simply varying the reactant concentrations. A dual template synergistically controlled micelle self-aggregated model was proposed to understand the formation mechanism of dendritic MSNs. In this model, the anionic surfactant stabilized micelles or micelle blocks are basic self-assembling build-

Table 1 Formation of cyclohexane oxide (CHO) from cyclohexene using different catalysts

Catalyst	Si/Ti	CHO yield/%	CHO sel/%	TOF/h^{-1}
Ti-DMSNs	42	25.1	95.7	63.3
Ti-MCM-41	45	22.9	96.2	61.8
TS-1	40	0.2	95.6	0.5

Reaction conditions: Catalyst, 50 mg; MeCN, 10 mL; cyclohexene, 10 mmol; TBHP (5.5 M in decane), 10 mmol; temp., 333 K; time, 2 h. The molar ratio of Si/Ti determined by ICP. Cyclohexene oxide (CHO). Turnover frequency (TOF): the amount of cyclohexene converted per Ti site per hour.

ing units for the formation of centre-radial pore channel networks. Ti-DMSNs synthesized by isomorphous substitution show a superior catalytic performance in the epoxidation of cyclohexene over titanosilicate microporous zeolites. The present mechanism paves the way for novel syntheses of other oxide nanomaterials, and novel applications in catalysis, energy conversion and nanomedicine.

Conflicts of interest

There are no conflicts to declare.

Acknowledgements

This work was supported by the NSFC (21373004, 21573074, 21776295 and 21533002), the CAS key laboratory of Low-Coal Conversion Science & Engineering and the JoRISS project.

Notes and references

1 V. Valtchev and L. Tosheva, *Chem. Rev.*, 2013, **113**, 6734–6760.

2 S.-H. Wu, C.-Y. Mou and H.-P. Lin, *Chem. Soc. Rev.*, 2013, **42**, 3862–3875.

3 L. Han and S. Che, *Chem. Soc. Rev.*, 2013, **42**, 3740–3752.

4 C. Gao and S. Che, *Adv. Funct. Mater.*, 2010, **20**, 2750–2768.

5 X. Du and S. Z. Qiao, *Small*, 2015, **11**, 392–413.

6 K. Moeller and T. Bein, *Chem. Mater.*, 2017, **29**, 371–388.

7 Y. Wan and D. Y. Zhao, *Chem. Rev.*, 2007, **107**, 2821–2860.

8 Y. Chen, H.-R. Chen and J.-L. Shi, *Acc. Chem. Res.*, 2014, **47**, 125–137.

9 E. Yamamoto, S. Mori, A. Shimojima, H. Wada and K. Kuroda, *Nanoscale*, 2017, **9**, 2464–2470.

10 E. Yamamoto and K. Kuroda, *Bull. Chem. Soc. Jpn.*, 2016, **89**, 501–539.

11 V. Polshettiwar, D. Cha, X. Zhang and J. M. Basset, *Angew. Chem., Int. Ed.*, 2010, **49**, 9652–9656.

12 D. Shen, J. Yang, X. Li, L. Zhou, R. Zhang, W. Li, L. Chen, R. Wang, F. Zhang and D. Zhao, *Nano Lett.*, 2014, **14**, 923–932.

13 X. Guo, Y. Deng, B. Tu and D. Zhao, *Langmuir*, 2010, **26**, 702–708.

14 Q. Yue, J. Li, W. Luo, Y. Zhang, A. A. Elzatahry, X. Wang, C. Wang, W. Li, X. Cheng, A. Alghamdi, A. M. Abdullah, Y. Deng and D. Zhao, *J. Am. Chem. Soc.*, 2015, **137**, 13282–13289.

15 D.-S. Moon and J.-K. Lee, *Langmuir*, 2012, **28**, 12341–12347.

16 X. Du and J. He, *Langmuir*, 2010, **26**, 10057–10062.

17 H. Zhang, Z. Li, P. Xu, R. Wu and Z. Jiao, *Chem. Commun.*, 2010, **46**, 6783–6785.

18 A. J. Paula, L. A. Montoro, A. G. S. Filho and O. L. Alves, *Chem. Commun.*, 2012, **48**, 591–593.

19 C. Pereira, C. Alves, A. Monteiro, C. Magén, A. M. Pereira, A. Ibarra, M. R. Ibarra, P. B. Tavares, J. P. Araújo, G. Blanco, J. M. Pintado, A. P. Carvalho, J. Pires, M. F. R. Pereira and C. Freire, *ACS Appl. Mater. Interfaces*, 2011, **3**, 2289–2299.

20 M. Wu, Q. Meng, Y. Chen, Y. Du, L. Zhang, Y. Li, L. Zhang and J. Shi, *Adv. Mater.*, 2015, **27**, 215–222.

21 A. B. D. Nandiyanto, S.-G. Kim, F. Iskandar and K. Okuyama, *Microporous Mesoporous Mater.*, 2009, **120**, 447–453.

22 K. Zhang, L.-L. Xu, J.-G. Jiang, N. Calin, K.-F. Lam, S.-J. Zhang, H.-H. Wu, G.-D. Wu, B. Albela, L. Bonneviot and P. Wu, *J. Am. Chem. Soc.*, 2013, **135**, 2427–2430.

23 Y.-J. Yu, J.-L. Xing, J.-L. Pang, S.-H. Jiang, K.-F. Lam, T.-Q. Yang, Q.-S. Xue, K. Zhang and P. Wu, *ACS Appl. Mater. Interfaces*, 2014, **6**, 22655–22665.

24 S. Yang, X. Zhou, P. Yuan, M. Yu, S. Xie, J. Zou, G. Q. Lu and C. Yu, *Angew. Chem., Int. Ed.*, 2007, **46**, 8579–8582.

25 H. Chen and J. He, *Chem. Commun.*, 2008, 4422–4424.

26 Y. Zhang, G. Zhou, B. Sun, M. Zhao, J. Zhang and F. Chen, *Chem. Commun.*, 2014, **50**, 2907–2909.

27 Y.-Q. Yeh, B.-C. Chen, H.-P. Lin and C.-Y. Tang, *Langmuir*, 2006, **22**, 6–9.

28 J. Wang, W. Xiao, J. Wang, J. Lu and J. Yang, *Mater. Lett.*, 2015, **142**, 269–272.

29 F. Gai, T. Zhou, G. Chu, Y. Li, Y. Liu, Q. Huo and F. Akhtar, *Dalton Trans.*, 2016, **45**, 508–514.

30 C. Urata, Y. Aoyama, A. Tonegawa, Y. Yamauchi and K. Kuroda, *Chem. Commun.*, 2009, 5094–5096.

31 Y. Zhou and M. Antonietti, *J. Am. Chem. Soc.*, 2003, **125**, 14960–14961.

32 M. Thommes, K. Kaneko, A. V. Neimark, J. P. Olivier, F. Rodriguez-Reinoso, J. Rouquerol and K. S. W. Sing, *Pure Appl. Chem.*, 2015, **87**, 1051–1069.

33 J. C. Groen, L. A. A. Peffer and J. Perez-Ramirez, *Microporous Mesoporous Mater.*, 2003, **60**, 1–17.

34 C. Weidenthaler, *Nanoscale*, 2011, **3**, 792–810.

35 J. Chaignon, Y. Bouizi, L. Davin, N. Calin, B. Albela and L. Bonneviot, *Green Chem.*, 2015, **17**, 3130–3140.

36 H. Duan, D. Wang and Y. Li, *Chem. Soc. Rev.*, 2015, **44**, 5778–5792.

37 M. C. Chao, H. P. Lin, C. Y. Mou, B. W. Cheng and C. F. Cheng, *Catal. Today*, 2004, **97**, 81–87.

38 T. Yokoi, T. Karouji, S. Ohta, J. N. Kondo and T. Tatsumi, *Chem. Mater.*, 2010, **22**, 3900–3908.

39 J. Wang, L. Xu, K. Zhang, H. Peng, H. Wu, J.-G. Jiang, Y. Liu and P. Wu, *J. Catal.*, 2012, **288**, 16–23.